

Thermal characteristics of Fabry–Perot cavity based on regenerated fiber Bragg gratings

Yumin Zhang (张钰民)¹, Yue Ren (任越)¹, Mingli Dong (董明利)^{2,*},
Fanyong Meng (孟凡勇)¹, and Lianqing Zhu (祝连庆)^{1,**}

¹Beijing Engineering Research Center of Optoelectronic Information and Instrument, Beijing Information Science and Technology University, Beijing 100016, China

²Beijing Key Laboratory of Optoelectronic Measurement Technology, Beijing Information Science and Technology University, Beijing 100192, China

*Corresponding author: dongml@bistu.edu.cn; **corresponding author: zhulianqing@sina.com

Received August 8, 2018; accepted October 24, 2018; posted online November 27, 2018

The Letter reports the thermal stability and strain response of Fabry–Perot (FP) cavity under different high temperatures. The FP cavity was made by thermal regeneration of two identical cascaded fiber Bragg gratings (FBGs). It is demonstrated that the FP cavity is capable of measuring temperatures from 300°C to 900°C with a temperature sensitivity of 15.97 pm/°C. The elongation of the fiber was observed through the drifted Bragg wavelength at 700°C or above when weight was loaded. The elongation was further inferred by the slight change in the interference spectra of the FP cavity at 900°C.

OCIS codes: 060.2370, 060.3735.
doi: 10.3788/COL201816.120601.

A fiber Bragg grating (FBG) is a kind of sensing element characterized by wavelength demodulation, small size, and flexible bend. It has been extensively used in various fields, such as bridge health monitoring^[1], wind turbine rotor blade^[2], railways^[3,4], urban infrastructure^[5], and medical applications^[6]. But beyond that, FBG sensors are capable of working well in harsh environments; for instance, they can be found in the fields of aircraft structure^[7], nuclear power plant^[8], and oil and gas transportation for structural health monitoring^[9].

Generally, FBGs could be achieved in two ways: one is the ultraviolet (UV) laser inscription method, and the other is based on infrared (IR) femtosecond (fs) laser pulse radiation. IR fs-induced FBGs can be written through various coatings, such as acrylate, polyimide, and carbon^[10]. Writing with IR fs pulses relies on a multi-photon process, which has the significant advantages of high strength, high reliability, and being the focus of research in recent years^[11–13]. Some excellent groups have reported that IR fs FBGs could be operated up to 1200°C with silica-based fibers and 1745°C with sapphire fibers^[14,15]. But, the cost of material and time for IR fs FBGs is relatively higher than that of conventional UV-induced FBGs. Therefore, the UV FBG still has great development and market potential in traditional sensing areas.

However, the UV-induced refractive change in the optical fiber core may degrade at temperatures higher than 300°C^[16]. Many efforts have been made to improve the temperature limit of silica fiber FBGs. Guan *et al.*^[17] provided a post-UV treated method to generate a high-temperature-resistant FBG that could survive at about 528°C. Bartelt *et al.*^[18] reported a type II FBG with a stable temperature response at 700°C. Oliveira *et al.*^[19] showed enhanced thermal stability at 800°C with

nonhydrogenated fibers. Chemical composition grating, namely the regenerated FBG, is also another way of pursuing better resistance at high temperatures for UV-written FBGs, which was first reported, to the best of our knowledge, by Fokine *et al.* in 2002^[20]. Several researchers have put a lot of work into regenerated FBGs for temperature and strain sensing^[21,22]. The theories of seeded crystallization and trapped water molecules are two representative different opinions^[23]. Up to now, the mechanism underlying the regeneration process is still inconclusive. Yet, it does not hold back the study of regenerated FBGs, but opens a new situation of rapid development.

Former researchers could observe the elongation of fibers under high-temperature strain at the end of the experiment^[24]. In this Letter, the tiny elongation could be monitored in real time and deduced from spectra during the experiment. Herein, two identically seeded FBGs were used for the regenerating process. After the regeneration, two cascaded FBG arrays were obtained, forming a micro-fiber Fabry–Perot (FP) interferometer. The regenerated FBGs were used for measuring the wavelength drift as the temperature changes, and the FP cavity would be capable of monitoring the strain response on line when the load was applied on the fiber at high temperatures.

The cascaded FBGs were inscribed by a beam scanning method combining phase mask technology. The UV laser used in the inscription is an argon ion laser (Coherent Innova 300C MOTOFRED) with an emission wavelength of 244 nm. The Bragg condition for an FBG is given by

$$\lambda_B = 2n_{\text{eff}} \cdot \Lambda, \quad (1)$$

where λ_B is the Bragg wavelength, n_{eff} is the effective refractive index of the fiber core, and Λ is the period of

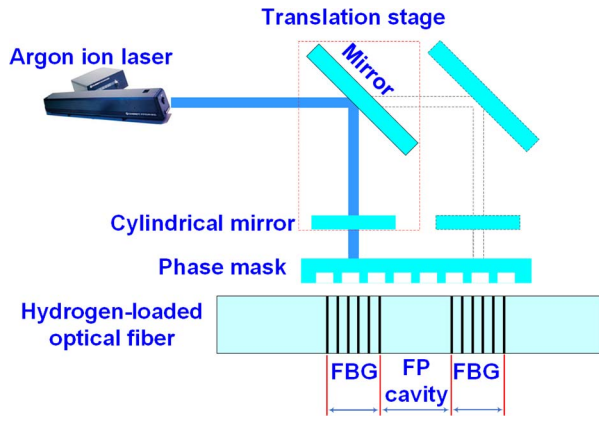


Fig. 1. Scheme for the setup of FBG inscription via the beam scanning method.

grating. Figure 1 shows the setup of FBG inscription. A UV reflective mirror and a cylindrical mirror were mounted on a high-precision translation stage with a minimum incremental motion of 1 nm (Newport XMS160). The UV circular beam was shaped into an ellipse with a long axis of 3 mm at the focal length of the cylindrical mirror. An interference pattern was created by two outgoing beams, which were produced by the first-order diffraction of the phase mask. When a hydrogen-loaded optical fiber was placed into the interference region adjacent to the phase mask, a periodical modulation occurred in the core of the optical fiber. If the proper velocity of the translation stage was controlled for the first exposure and followed by the second exposure without a phase mask, a kind of apodized FBG could be obtained. The length and transmission depth of the FBG can be adjusted by controlling the moving distance of the translation stage and the exposure time. Here, a Corning HI1060 FLEX optical fiber was used for inscription after hydrogen loading ($P = 1950$ psi, $T = 80^\circ\text{C}$, $t = 7$ days). Two identical FBGs were fabricated via the above-mentioned method. The two FBGs have the same length of 8 mm. The length of the FP cavity induced by FBGs is 9 mm. The spectrum of the reflected light was recorded by an optical spectrum analyzer (Yokogawa AQ6370D). The reflection and transmission spectra of the two FBGs are shown in Fig. 2. The first FBG has a transmission depth of 40 dB with a 3 dB reflection bandwidth of 0.7314 nm, as shown in Fig. 2(a). After the second inscription, the transmission depth of the cascaded FBGs is approximately 47.25 dB, and the 3 dB reflection bandwidth becomes 0.9467 nm, as shown in Fig 2(b). The cascaded FBGs were placed in air for subsequent use.

The regeneration and temperature response of FBGs were evaluated by placing the cascaded FBGs inside a muffle furnace. The thermal regeneration processing recipe for the cascaded FBGs is shown in Fig. 3. Firstly, the temperature was increased from room temperature to 900°C within 40 min. For a dwell time of 1.5 h at 900°C , the cascaded FBGs experienced spectral degeneration and regeneration completely. The red curve in Fig. 4 displays

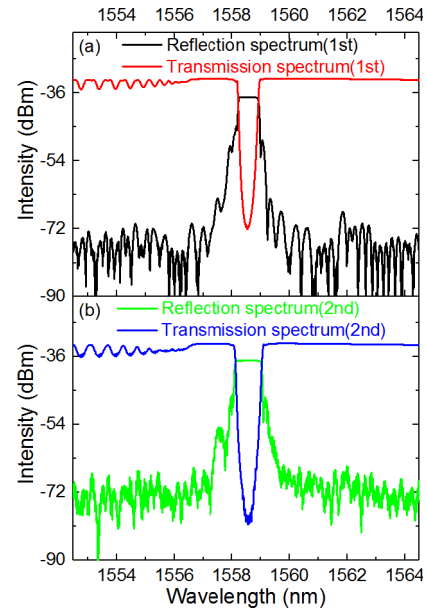


Fig. 2. Reflectance and transmittance spectra of the identical FBGs.

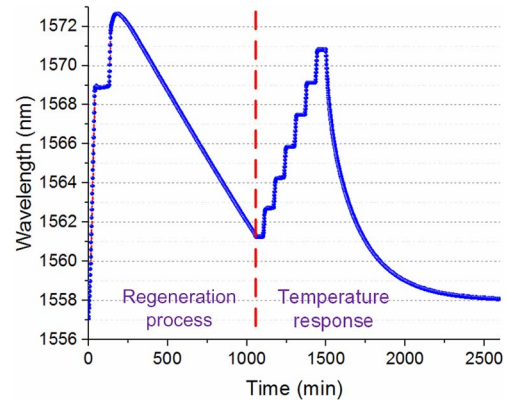


Fig. 3. Wavelength evolution of the cascaded FBGs during the regeneration and temperature response.

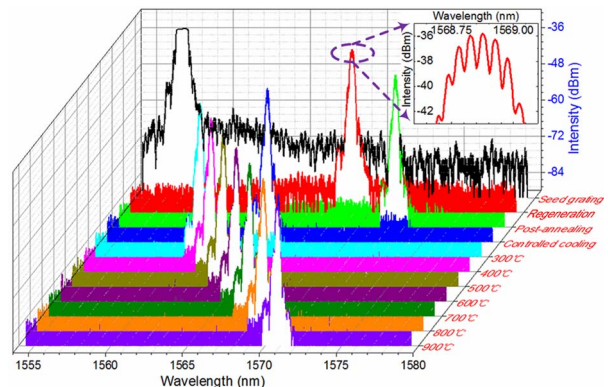


Fig. 4. Reflective spectra of the cascaded FBGs during the regeneration and temperature response. The inset is the partial enlargement of the spectrum after the regeneration.

the spectrum of the regenerated FBGs. It can be clearly seen that the interference pattern forms in the spectral profile of the FBG, as shown in the drawing of the partial enlargement in Fig. 4. Secondly, the temperature rose to 1050°C within 10 min and lasted for a period of 20 min so as to finish the post-annealing procedure. Thirdly, the temperature was set from 1050°C to 300°C with a controllable cooling rate of 50°C/h. Finally, the furnace was heated from 300°C to 900°C with a temperature interval of 100°C. At each temperature holding point, the dwell time was 1 h. After that, the furnace naturally cooled down. The post-annealing and controlled cooling would be helpful to stabilize the regenerated FBGs. It is indicated by the stable wavelength at each holding point, as shown in Fig. 3. Moreover, Fig. 4 describes the good shape of the reflective spectra from 300°C to 900°C. It means that the two identical FBGs were regenerated simultaneously and formed a kind of FP interferometer.

Figure 5 depicts the temperature dependence of the wavelength for the regenerated FBGs. The reflective spectrum splits into multi-peaks due to the interference by the FBG-induced FP cavity. A 10 dB spectrum width method was used to evaluate the central wavelength of the multi-peaks spectrum^[25], as shown in the inset of Fig. 5. The central Bragg wavelength of the cascaded FBGs can be obtained from the following equation:

$$\lambda_c = (\lambda_1 + \lambda_2)/2, \quad (2)$$

where λ_c is the central Bragg wavelength, and λ_1 and λ_2 are the left and right wavelengths corresponding to the 10 dB bandwidth of the spectrum profile, respectively. The slope of the temperature response is related to the thermo-optics and thermal-expansion coefficients. It is indicated that the wavelength kept a linear relationship with the temperature. The slope is 15.97 pm/°C, and the correlation coefficient is 0.999. It means that the regenerated FBGs could be competent to measure temperatures within 900°C.

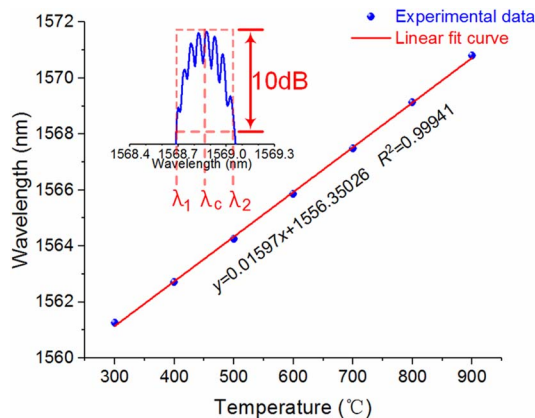


Fig. 5. Temperature dependence of the wavelength for the regenerated FBGs from 300°C to 900°C. The inset shows the method to obtain the Bragg wavelength of the cascaded FBGs.

The high-temperature strain response was performed in the muffle furnace with the regenerated FBGs under a load of 51.37 g, which is equivalent to $\sim 570 \mu\epsilon$. The temperature of the muffle furnace was set from 300°C to 900°C with a temperature interval of 100°C, and the holding time lasted for about 1 h. The reflective spectra were recorded by the optical spectrum analyzer. The central wavelength was acquired with the above-mentioned method. The wavelength evolution was depicted in Fig. 6. It can be seen that the wavelength drift is not obvious below the temperature of 600°C. But, when the temperature rose to 700°C or above, the wavelength appeared with an apparent red shift. The wavelength drift at 700°C is about 32 pm, whereas the drift is 77 pm at 800°C. Furthermore, for the sake of obviousness, the dwell time at 900°C lasted for 3 h. The wavelength drift reaches up to 1.4 nm. As for the 900°C, the reflective spectra were thoroughly analyzed, as shown in Fig. 7. In a linear scale, the reflective spectrum has three peaks at the beginning, and four peaks emerge at the end of 3 h, as shown in Fig. 7(a). Figure 7(b) displays the specific spectral evolution at different times at 900°C. It is known that if the length of the FP cavity becomes longer, the period of interference fringes gets shorter^[26]. Therefore, it is deduced that the cavity length formed by identical FBGs has been stretched. In other words, the optical fiber is elongated under high-temperature strain. It is consistent with the previously reported phenomenon^[27,28].

It must be admitted that the speed of elongation for the optical fiber at 900°C is not very fast. Both the reflectivity and 10 dB bandwidth of the FP cavity remain nearly constant. For the sake of understanding the high-temperature strain response of the FP cavity, higher temperature was provided. The temperature of the muffle furnace rose up to 1000°C from 900°C within 10 min and then lasted for about 25 min. It was found that the 10 dB bandwidth gradually became wider with the temperature rising and holding, as shown in Fig. 8. Particularly, the bandwidth increased by 0.23 nm within 25 min at 1000°C. The reflective spectrum remained normal at the beginning

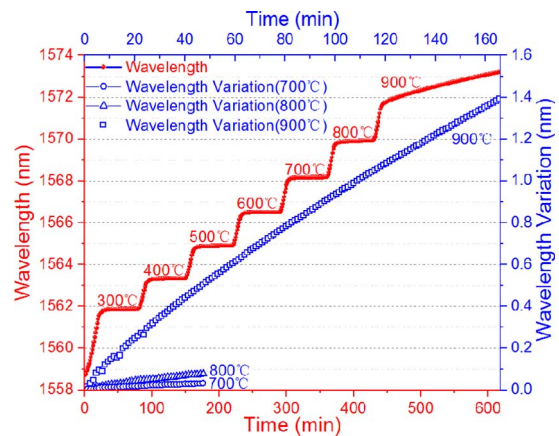


Fig. 6. Wavelength evolution of regenerated FBGs under high-temperature strain.

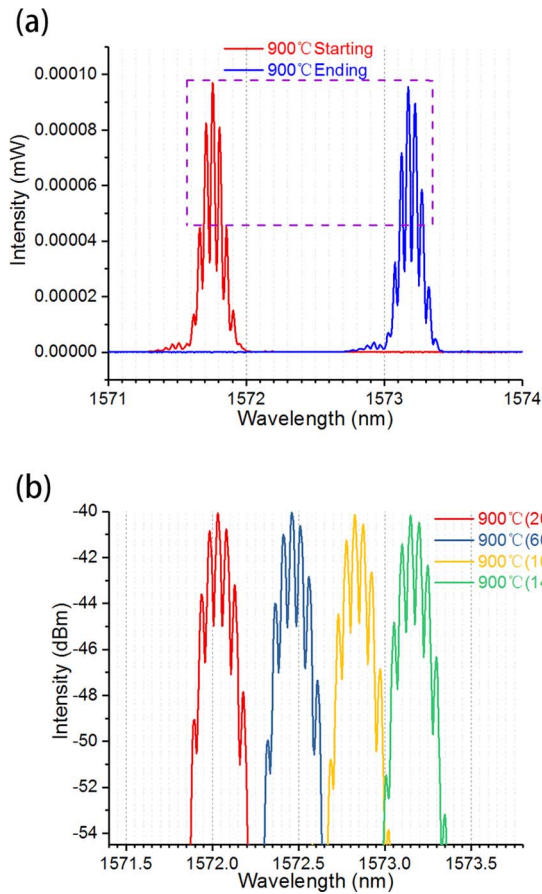


Fig. 7. Reflective spectra of regenerated FBGs at 900°C under strain. (a) Starting and ending with the linear scale. (b) Process with the logarithmic scale.

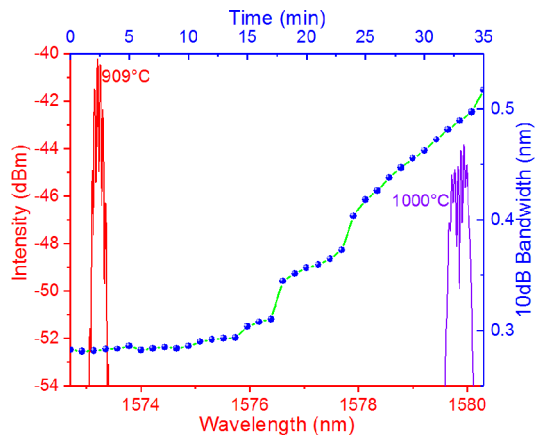


Fig. 8. Time dependence of 10 dB bandwidth for the regenerated FBGs from 900°C to 1000°C and reflective spectra at 909°C and 1000°C.

of the temperature rising; however, the wave profile of the FP cavity split apart into two peaks at the end of the temperature holding, as shown in Fig. 8. The intensity of the reflection peak has sharply declined. It is due to the period-length mismatch between the two FBGs of the FP cavity under high temperatures. As for the germanium-doped optical fiber, the drawing tension mainly results

from the cladding, whereas the stress arising in the core is negligible^[28]. Therefore, the residual stress is concentrated at the cladding. When the FP cavity was annealed at 1000°C for 25 min, the residual stress at cladding was released. However, the residual stress release was uncontrollable, which gave rise to the mismatch between the identical FBGs. Then, the rigid FP cavity was destroyed, and split peaks were formed. It means that a higher temperature could accelerate the elongation of the optical fiber under loading or even destroy the intrinsic properties of the optical fiber produced by the drawing tower.

In conclusion, the inscription of identical FBGs was achieved via the beam scanning method combined with phase mask technology. An FP interferometer was obtained after the thermal regeneration of the cascaded FBGs. The FP cavity showed a linear temperature dependence of the Bragg wavelength from 300°C to 900°C, and the temperature sensitivity was 15.97 pm/°C. It was also indicated that the FP cavity could be capable of responding to high-temperature strain, and the elongation of the optical fiber was indirectly verified.

This work was supported by the Program for Changjiang Scholars and Innovative Research Team in the University of Ministry of Education of China (No. IRT_16R07) and the Importation and Development of High-Caliber Talents Project of Beijing Municipal Institutions (No. IDHT20170510). We thank the Beijing Laboratory of Optical Fiber Sensing and System for the use of their equipment. We thank Prof. Zhu for assistance with financial support.

References

1. X. Kong, S. C. M. Ho, G. S. Song, and C. S. Cai, *J. Bridge Eng.* **22**, 11 (2017).
2. H. I. Kim, J. H. Han, and H. J. Bang, *Wind Energy* **17**, 451 (2014).
3. S. J. Buggy, S. W. James, S. Staines, R. Carroll, P. Kitson, D. Farrington, L. Drewett, J. Jaiswal, and R. P. Tatam, *Meas. Sci. Technol.* **27**, 055201 (2016).
4. X. Wang, Y. Guo, and L. Xiong, *Chin. Opt. Lett.* **16**, 070604 (2018).
5. H. F. Lima, R. D. Vicente, R. N. Nogueira, I. Abe, P. S. Andre, C. Fernandes, H. Rodrigues, H. Varum, H. J. Kalinowski, A. Costa, and J. D. Pinto, *IEEE Sensors J.* **8**, 1236 (2008).
6. Z. Liu and H. Y. Tam, *Chin. Opt. Lett.* **14**, 120007 (2016).
7. M. Mieloszyk, M. Krawczuk, A. Zak, and W. Ostachowicz, *Smart Mater. Struct.* **19**, 085009 (2010).
8. L. Remy, G. Cheymol, A. Gusarov, A. Morana, E. Marin, and S. Girard, *IEEE Trans. Nucl. Sci.* **63**, 2317 (2016).
9. X. G. Qiao, Z. H. Shao, W. J. Bao, and Q. Z. Rong, *Sensors* **17**, 34 (2017).
10. S. K. Ibrahim, J. A. O'Dowd, V. Bessler, D. M. Karabacak, and J. M. Singer, *Proc. SPIE* **10208**, 102080P (2017).
11. D. Grobnic, C. W. Smelser, S. J. Mihailov, R. B. Walker, and P. Lu, *IEEE Photon. Technol. Lett.* **16**, 1864 (2004).
12. X. Fang, C. R. Liao, and D. N. Wang, *Opt. Lett.* **35**, 1007 (2010).
13. S. Yang, D. Hu, and A. B. Wang, *Opt. Lett.* **42**, 4219 (2017).
14. Y. H. Li, M. W. Yang, D. N. Wang, J. Lu, T. Sun, and K. T. V. Grattan, *Opt. Express* **17**, 19785 (2009).

15. M. Busch, W. Ecke, I. Latka, D. Fischer, R. Willsch, and H. Bartelt, *Measure. Sci. Technol.* **20**, 115301 (2009).
16. S. R. Baker, H. N. Rourke, V. Baker, and D. Goodchild, *J. Lightwave Technol.* **15**, 1470 (1997).
17. B. O. Guan, H. Y. Tam, C. Lu, and X. Y. Dong, *IEEE Photon. Technol. Lett.* **13**, 591 (2001).
18. H. Bartelt, K. Schuster, S. Unger, C. Chojetzki, M. Rothhardt, and I. Latka, *Appl. Opt.* **46**, 3417 (2007).
19. V. Oliveira, M. Muller, and H. J. Kalinowski, *Appl. Opt.* **50**, E55 (2011).
20. M. Fokine, *Opt. Lett.* **27**, 1016 (2002).
21. H. Z. Yang, X. G. Qiao, Y. P. Wang, M. M. Ali, M. H. Lai, K. S. Lim, and H. Ahmad, *IEEE Photon. Technol. Lett.* **27**, 58 (2015).
22. X. W. Shu, D. H. Zhao, L. Zhang, and I. Bennion, *Appl. Opt.* **43**, 2006 (2004).
23. P. Holmberg, F. Laurell, and M. Fokine, *Opt. Express* **23**, 27520 (2015).
24. L. Y. Shao, J. Canning, T. Wang, K. Cook, and H. Y. Tam, *Acta Mater.* **61**, 6071 (2013).
25. Y. Li, N. Kuse, A. Rolland, Y. Stepanenko, C. Radzewicz, and M. E. Fermann, *Opt. Express* **25**, 18017 (2017).
26. C. R. Liao, T. Y. Hu, and D. N. Wang, *Opt. Express* **20**, 22813 (2012).
27. T. Wang, L. Y. Shao, J. Canning, and K. Cook, *Appl. Opt.* **52**, 2080 (2013).
28. Y. Hibino, F. Hanawa, and M. Horiguchi, *J. Appl. Phys.* **65**, 30 (1989).